Influence of Surfactant-Cosurfactant Ratios on the Morphology of Vaterite Microparticles in Inverse Microemulsions

Meikun Hu,^[a] Ke Wang,^[a] Jiajun Zuo,^[a] Martyn Jevric*^[b], Jiaming Feng^[a], Zhihang Wang*^[c,d] and Nong Wang*^[a]

^[a] School of Chemistry and Chemical Engineering, Lanzhou Jiaotong University, Lanzhou, 730070, People's Republic of China

[b] School of Rural Medicine, University of New England, Armidale, NSW, 2351, Australia

^[c] School of Engineering, College of Science and Engineering, University of Derby, Markeaton Street, Derby DE22 3AW, United Kingdom

^[d] Department of Materials Science and Metallurgy, University of Cambridge, 27 Charles Babbage Road, Cambridge, CB3 0FS, United Kingdom

ABSTRACT: The controlled growth of calcium carbonate microcrystals is essential for their use in various industries such as construction, plastics, and textiles, where specific mineral forms and morphologies are required. A common method to achieve desired morphologies involves the use of surfactants to encapsulate calcium salts in a microemulsion environment (for instance, water in oil) to facilitate the growth of the microcrystals. In our work, we employed a system comprising octyl phenol ether-10 as the surfactant and n-heptanol as the co-surfactant. This mixing approach effectively fine-tuned the shape formation of vaterite calcium carbonate microcrystals. The study emphasizes the crucial role of surfactant and cosurfactant ratios in oil-in-water inverse emulsions for the generation of microparticles in diverse shapes. It was found that a higher ratio of octyl phenol ether-10 to n-heptanol (4:1) results in the formation of needle-shaped vaterite microparticles, whereas a lower ratio (1:1) leads to coral-shaped structures, together with a variety of shapes observed at intermediate

 $\textit{E-mail addresses:} \ \ \text{mjevric@une.edu.au} \ (M.\ Jevric); \ z. wang@derby.ac.uk \ (Zhihang\ Wang); \ wangnong 07@163.com \ (Nong\ Wang).$

^{*} Corresponding author.

^{**} Correspondence to: N. Wang (+86-13893617023), School of Chemistry and Chemical Engineering, Lanzhou Jiaotong University, Lanzhou 730070, P. R. China

ratios. Theoretical calculations, based on improved critical packing parameter theory, were conducted to shed light on the mechanisms behind these morphological variations. This method opened new avenues in mineral crystal growth and surface engineering.

Keywords: coral-like, calcium carbonate, inverse microemulsion, improved critical packing parameters theory

1. Introduction

Calcium carbonate (CaCO₃), widely abundant in nature, [1, 2] is a key component of biomineralization. [3-6] This resource exists in six polymorphic forms: the amorphous structure, hydrated crystalline phases like hexahydrate ikaite and monohydrocalcite, and anhydrous crystals including vaterite, aragonite, and calcite.^[7-9] For instance, vaterite, a metastable hexagonal crystalline structure often found in spherulitic or disc-like forms, serves as a precursor to calcite and aragonite.^[10] Calcite, in contrast, is the most stable form of CaCO₃.^[11] Beyond varying crystal packing, calcium carbonate particles also exhibit diverse morphologies such as cubic, needle, chain, spindle, and spherical shapes. The physical properties and specific applications of these particles are heavily influenced by their distinct shapes. Widely utilized in industries like rubber, [12, 13] plastics, [14] ink production,^[15] coatings,^[16, 17] and papermaking.^[18] As examples, CaCO₃ particles in cube shape are desirable in industries as papermaking and paint making. As a reinforcing material, the cubic calcite particles may yield high smoothness and excellent gloss to the composite since they are easily aligned in a regular way. They may also yield high electric insulation and elasticity modulus to the composite. [19] Needle-shaped particles offer a significant advantage by providing a high aspect ratio, which enhances the bending and impact strength of plastics and rubber materials. In particular, aragonite whiskers have proven to be superior to calcite as fillers in polyvinyl or polypropylene composites. The incorporation of aragonite whiskers into these composites results in improved tensile strength, impact strength, glass transition temperature, and decomposition temperature.^[14] To ensure optimal compatibility between the aragonite whiskers and the rubber matrix, surface alteration techniques are employed. This surface modification enhances various properties, including the pyane effect, storage modulus, and overall physical characteristics of the composites.^[20] Spherical calcium

carbonate particles possess excellent dispersibility and abrasion resistance, where they can improve viscosity, stability, and drying speed. [21-23] Additionally, due to their unique properties, such as high surface area and chemical stability, spherical nano-sized calcium carbonate particles are utilized in the fields of drug delivery, ceramics and orthopedic. [24-26] Recognizing that the size and shape of CaCO₃ crystals are key determinants of their properties and applications, substantial research efforts are dedicated to developing reliable methods for controlling the morphology and size of CaCO₃ microparticles. [27-30]

Emulsions, frequently used to encapsulate organic compounds in solutions, typically comprise at least two immiscible liquids, such as oil and water. In these systems, one liquid is dispersed as tiny droplets within the other.^[31] Depending on which phase (oil or water) is dispersed, emulsions are classified as oil-in-water (O/W)^[32] or water-in-oil (W/O).^[33] Additionally, there are complex multiple emulsions, like oil-in-water-in-oil (O/W/O) or water-in-oil-in-water (W/O/W) emulsions. [34, 35] To stabilize these mixtures, emulsifiers are added, creating a kinetically stable system. [36] The formation, stability, and properties of these emulsions depend heavily on the characteristics of the oil phase (such as polarity, water solubility, viscosity, density) and the nature and concentration of components in the aqueous phase. [37] In this context, the choice of surfactant for use as an emulsifier is of paramount importance. Microemulsions, sometimes also referred to as nanoemulsions, [38] are thermodynamically stable and isotropic transparent emulsions with droplet diameter of 20 to 200 nm. They are heterogeneous dispersions of two immiscible phases of oil and water, and can be stabilized by interfacial layer of surfactants and cosurfactants. Today, with the development of various intelligent composite materials, [39] the microemulsion method is a commonly employed technique for producing nano or micro particles. [40, 41] In the realm of W/O microemulsions, commonly referred to as inverse microemulsions, small hydrophilic droplets, often termed "water pools", are encapsulated within a monolayer of emulsifiers consisting of surfactants and co-surfactants. The size of these pools can be easily regulated by adjusting the molar ratio of surfactant to water.^[42] This approach facilitates the creation of CaCO₃ particles in a variety of size through a simple process that eliminates the need for high-temperature calcination and allows for size customization.^[43] However, despite considerable research efforts, the control of polymorphism in CaCO₃ still largely depends on empirical methods.^[44] It is still a difficult task for controlling the shape and morphology of micro and nano particles.

In our study, we used an innovative inverse microemulsion system, employing a binary system of surfactant (polyoxyethylene octyl phenol ether-10, OP-10) and cosurfactant (n-heptanol), to fabricate CaCO₃ microparticles. Water-in-oil (W/O) inverse microemulsion systems were used rather than oil-in-water (O/W) because the CaCO₃ precipitation reaction occurs in the aqueous phase, where Ca²⁺ and CO₃²⁻ ions are soluble and reactive. Inverse microemulsions provide nanometer-scale water pools within the oil phase, offering a confined environment for controlled nucleation and growth. In contrast, O/W systems lack this spatial control, leading to rapid aggregation and poorly defined morphologies. Therefore, W/O microemulsions are more suitable for tailoring particle shape and size.

We discovered that while OP-10 is the principal surfactant for inverse emulsion, it could not easily form suitable inverse microemulsions for generating CaCO₃ particles. However, both OP-10 and n-heptanol exhibit excellent solubility in mixed solvents, effectively facilitating the formation of microemulsions, then to form CaCO₃ microparticles. The ratio of surfactant to cosurfactant was found to be crucial in producing a diverse range of shapes, from rods to coral-like structures. To decipher the mechanism behind this, the influence of the cosurfactant on micelle geometry was explored by improving critical packing parameters theory. This theory elucidated how the distribution of cosurfactant and surfactant molecules at the oil-water interface could modify the micellar geometry, thus influencing the shape of the initial CaCO₃ nanoparticles and, consequently, the microparticles' final form. Among the various shapes, the coral-like microparticles, with their large relative surface area, were identified as candidates for practical applications in hydrophobic surface coatings. As a demonstration, these coral-like particles were modified with stearic acid and subjected to surface contact angle testing to evaluate their hydrophobicity. The results showed excellent hydrophobic properties, akin to the natural surface of a lotus leaf, when compared to similarly modified cubic-shaped microparticles.

2. Experimental section

2.1. Materials

Chemicals used in this study were purchased from different sources: CaCl2 and ammonia were

supplied by Tianjin Damao Chemical Factory, China. Polyoxyethylene octyl phenol ether-10 (OP-10) and cyclohexane were provided by Shandong Shuangshuang Chemical Factory, China. *n*-Heptanol was purchased from Shanghai Rhawn Chemical Technology Co., Ltd, China. All these chemicals were analytical grade and used without further purification. Water was distilled prior to use.

2.2. Equipment and characterization

The size and morphology of the obtained CaCO₃ microparticle samples were analyzed by scanning electron microscopy (SEM; JSM-6100, JEOL Ltd, Japan; Quanta 650, FEG, FEI, America). Infrared spectroscopy was recorded by a Fourier transform infrared spectrometer (FTIR; EXUS–470, Nicolet, Japan). The crystal structure types were analyzed by powder X-ray diffraction (XRD; RINT-1000, Rigaku, Japan). The stability of CaCO₃ microparticles was studied by thermogravimetric analysis (TGA; TGA55, TA Instruments, America). Contact angle measurements of stearate coated microparticles were made using a video optical contact angle tester (CA; OCA25, Eastern-Dataphy, Germany). All the glassware and storage bottles were immersed in hydrochloric acid overnight, then rinsed thoroughly with distilled water as a cleaning procedure prior to being used in all experiments.

2.3. Preparation methods

The method for preparing coral-like micro-CaCO₃ comprised of the following steps: Calcium chloride (5.5 g) was dissolved in 25% aqueous ammonia (7 mL) and diluted with water to give a final volume of 100 mL. This aqueous solution, cyclohexane, *n*-heptanol, and OP-10 were combined to prepare a stable inverse microemulsion. The volume ratio used of the surfactant, cosurfactant, cyclohexane, and calcium chloride solution was 60mL: 60 mL: 200 mL: 16 mL. Here the volume ratio between the surfactant and cosurfactant (S/CoS) used were 1:1. To ensure consistency, carbon dioxide (CO₂) gas was then bubbled into the microemulsion at a fixed flow rate of 300 mL/min throughout all experiments. With the continuous penetration of CO₂, the microemulsion becomes turbid overtime, indicating the beginning of precipitation. CO₂ was further introduced for an additional 30 minutes under constant stirring to ensure sufficient reaction and complete particle formation. During the precipitation, the solution was continuously stirred at a constant rate of 650 r/min at room temperature for 30 min, after which time the CaCO₃ particles were allowed to age for

24 h. The final precipitation was dispersed in ethanol and centrifuged at 3000 r/min for 5 min. Such a process was repeated three times. After the last centrifugation, the particles were dried in the oven at 70 °C for 24 h. To examine the effect of the surfactant to cosurfactant (S/CoS) ratio, additional samples were prepared using the same procedure, except the volume ratios of S/CoS were varied as 4:1, 3:1, and 2:1.

2.4. Contact angle measurements and surface modification of coral-like microparticles with stearic acid

The surface modification method of coral-like microparticles and synthesis of cubic CaCO₃ microparticles has been reported in our previous paper.^[45] In this work, a 0.5 M stearic acid solution was diluted in n-hexane (10 mL) at 50 °C. Subsequently, coral-shaped CaCO₃ microparticles (2.0 g) were added to create a suspension, which was stirred for 30 minutes. The suspension was then dried at 70 °C to evaporate the n-hexane, yielding a final white powder. For contact angle measurements, approximately 5 mg of this dried powder was coated onto a glass slide using double-sided tape.

To evaluate the potential of coral-like CaCO₃ microparticles as hydrophobic coating materials, cubic CaCO₃ microparticles consisting of a mixture of calcite and vaterite with a relatively lower surface area were similarly prepared for comparison. For this, OP-10 (1.1 mL) and ethanol (9 mL) were mixed into a 50 ml 0.5M CaCl₂ solution in 25% aqueous ammonia. This mixture was stirred in open air for 10 hours and then allowed to stand for 48 hours at room temperature. The treatment process for preparing cubic-shaped CaCO₃ microparticles was analogous to that of the coral-like microparticles. A film derived from the modified cubic-shaped CaCO₃ microparticles was also prepared using the same method.

3. Results and discussion

3.1. Morphology

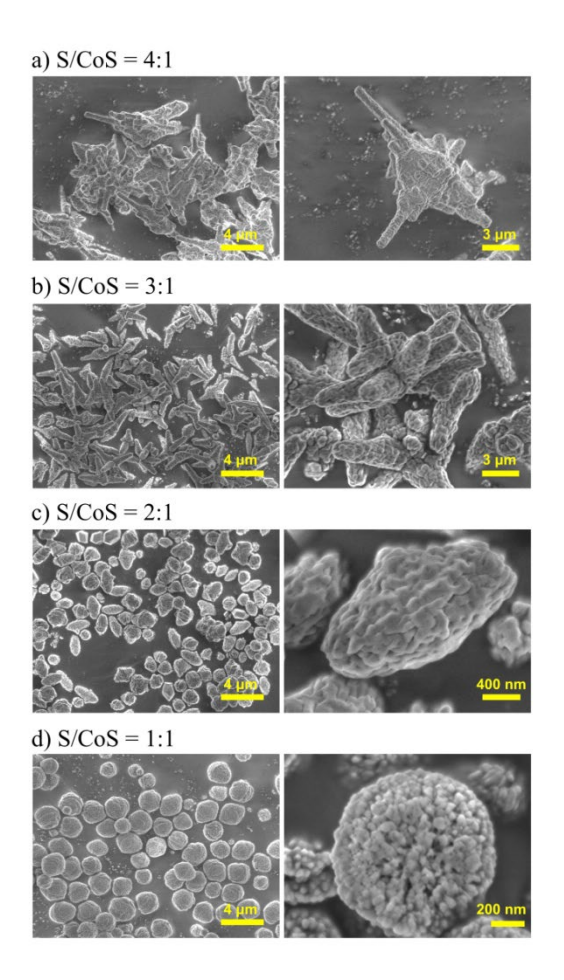


Figure 1. SEM images of CaCO₃ microparticles prepared under different S/CoS ratios (a: S/CoS=4:1, b: S/CoS=3:1, c: S/CoS=2:1, d: S/CoS=1:1) where S is surfactant OP-10, and CoS is co-surfactant *n*-heptanol.

Figure 1 highlights the SEM images of CaCO₃ microparticles prepared by the inverse microemulsion methodology. The morphology of CaCO₃ microparticles change in a trend from long rod (1a) to short rod (1b), then to ellipsoid (1c) and finally to spherical shape (1d) as the S/CoS decreased. When the volume ratio of S/CoS was 4:1, rod-shaped CaCO₃ about 0.5 μm wide and 10 μm long were obtained, Figure 1a shows their irregular aggregates. When S/CoS=3:1, similar shorter rod-shaped CaCO₃ particles were observed as shown in Figure 1b, which was about 0.5 μm wide but only 3 μm long. In contrast, when S/CoS=2:1, larger ellipsoidal shaped CaCO₃ particles with a length of about 1~2 μm were obtained (Figure 1c). Finally, when S/CoS=1:1, coral-like CaCO₃ microparticles can be obtained, which can be seen in Figure 1d. The particles exhibited a spherical

morphology with a diameter of approximately 2 μm. Their surface was adorned with numerous nanosized spheres, each measuring about 40-50 nm in diameter. By scanning this coral-like CaCO₃ sample (Figure 1d), very few hollow raspberry-like, and starfish-like CaCO₃ particles were found in using electron microscopy (Figure 2). This is likely to be coral-shaped microparticles with defects, due to an incomplete reaction or could it be that the CO₂ had been consumed prior to complete coral shaped microparticles' formation.

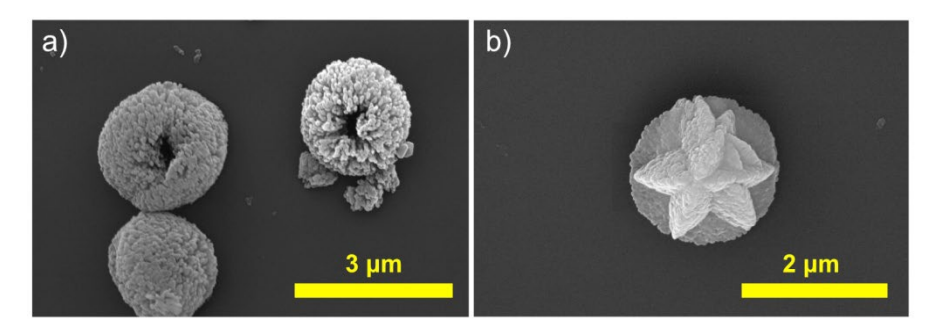


Figure 2. SEM images of a) raspberry-like CaCO₃ microparticles and b) starfish-like CaCO₃ microparticles made in this study.

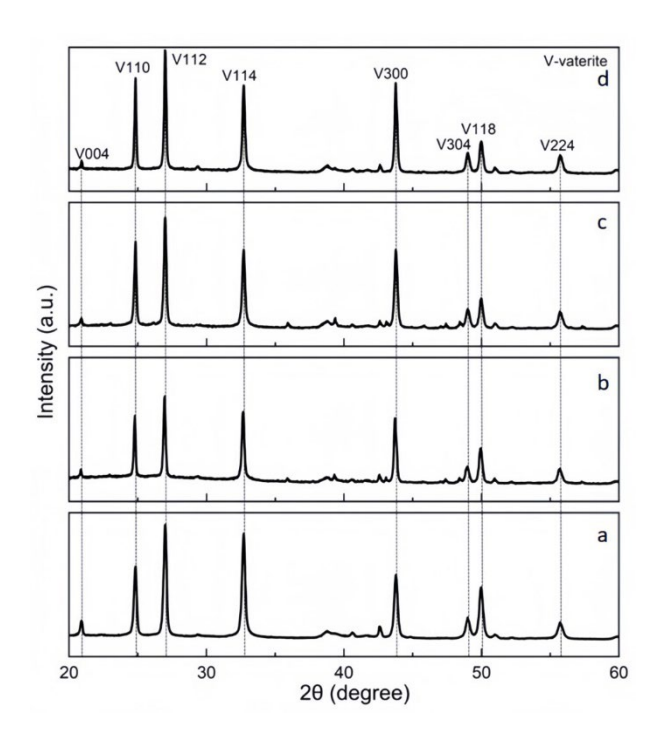


Figure 3. The XRD patterns of CaCO₃ particles (a: S/CoS=4:1, b: S/CoS=3:1, c: S/CoS=2:1, d: S/CoS=1:1).

3.2. Structure and crystal type determination using XRD, IR and TGA

At room temperature and atmosphere pressure, anhydrous calcium carbonate usually exists in the form of amorphous, calcite and vaterite. These structural forms can be distinguished conveniently using powder diffraction employing an X-ray source. To understand the structure and crystal type of the prepared $CaCO_3$ particle samples, XRD measurements were made on all the $CaCO_3$ microparticles made in this study and the diffraction patterns can be seen in Figure 3(a-d). Upon comparison of these diffraction patterns with all six known space groups, the data all match well with vaterite type crystal packing. Specifically, the diffraction peaks of 2θ at 20.87° , 24.82° , 26.96° , 32.67° , 43.77° , 48.99° , 49.98° , and 55.78° in Figure 3a correspond to (004), (110), (112), (114), (300), (304), (118), (224) crystal planes of the vaterite $CaCO_3$ particles. Interestingly, all batches prepared in this study displayed the same diffraction patterns, indicating that changing S/CoS ratio did not have an affect on the crystal packing of these different shaped $CaCO_3$ microparticles, only the shapes of the microparticles observed under SEM.

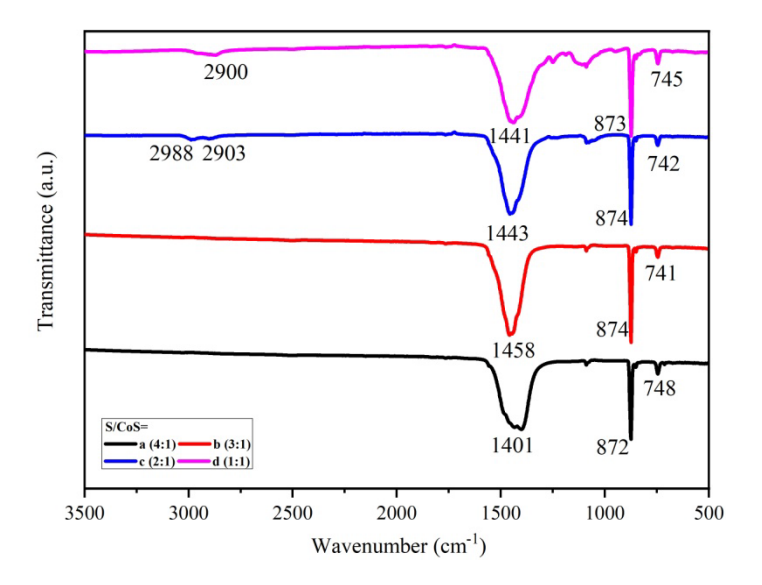


Figure 4. The FTIR spectra of CaCO₃ particles (a: S/CoS=4:1, b: S/CoS=3:1, c: S/CoS=2:1, d: S/CoS=1:1)

Figure 4 presents the infrared spectra of CaCO₃ microparticles synthesized at S/CoS ratios. In this figure, the wavenumber range from 500 to 3500 cm⁻¹, covering all vibronic features characteristic of all forms of CaCO₃, was thoroughly examined. The spectra of all samples exhibit a broad peak at 1401 cm⁻¹, indicative of the asymmetric stretching vibration of the C-O bond, characteristic of CaCO₃ particles. Additionally, the peak observed around 872 cm⁻¹ is likely due to the out-of-plane bending

vibration of the C-O bond. Notably, the distinct peak around 748 cm⁻¹ is attributed to the C-O asymmetric stretching vibration, a characteristic absorption peak unique to vaterite. These spectral features corroborate that all CaCO₃ microparticles produced in this study are vateritic, aligning with the findings from XRD measurements. In the spectra, additional weak features were observed at 2900 cm⁻¹ and 2988 cm⁻¹, attributed to O-H bond stretching vibrations. These features were notably present in samples 4c and 4d, prepared with larger quantities of the co-surfactant n-heptanol, but absent in samples 4a and 4b. This difference is likely due to the residual presence of n-heptanol or the cosurfactant OP-10, which possesses a terminal alcohol group. In samples 4c and 4d, these substances are likely trapped on the particle surfaces due to their high surface area, inhibiting their diffusion from the nanoparticles. In contrast, with S/CoS ratios of 4:1 and 3:1, there is less adsorption of n-heptanol and OP-10 on the CaCO₃ surfaces. However, when the S/CoS ratio is 2:1 or 1:1, the CaCO₃ particles exhibit better dispersibility and the presence of nano-sized particles on the microspheres' surfaces. This results in the CaCO₃ particle surfaces being more heavily coated with surfactants and cosurfactants.

Figure 5 presents the thermogravimetric (TG) analyses of four distinct CaCO₃ microcomposite materials. The observed weight loss can be categorized into two stages. The first stage, occurring between room temperature (25 °C) and 620 °C, shows a weight loss rate ranging from 2% to 4%. This stage is primarily due to the dehydration and carbonization of surfactants and cosurfactants adsorbed on the CaCO₃ particle surfaces. Furthermore, it was observed that CaCO₃ microparticles prepared with varying S/CoS ratios exhibited different weight losses during this stage. Specifically, a higher S/CoS ratio, as seen in long needle CaCO₃ microparticles (S/CoS = 4:1), corresponded to lower weight loss in the first stage (as detailed in Table 1). In contrast, lower S/CoS ratios, typical for corallike CaCO₃ microparticles (S/CoS = 1:1), led to more dispersed particles with smaller sizes, indicating a higher coating of surfactants and cosurfactants. Consequently, during heating, a greater amount of these substances carbonized, resulting in higher weight loss and a smaller quantity of residual calcium oxide in this stage. Therefore, coral-like CaCO₃ particles with an S/CoS ratio of 1:1, characterized by a relatively large surface area and extensive defects/cracks for improved dispersibility, were coated

with the highest amount of surfactants and cosurfactants. This also aligned with the highest weight loss rate observed, corroborating the findings from FTIR analyses.

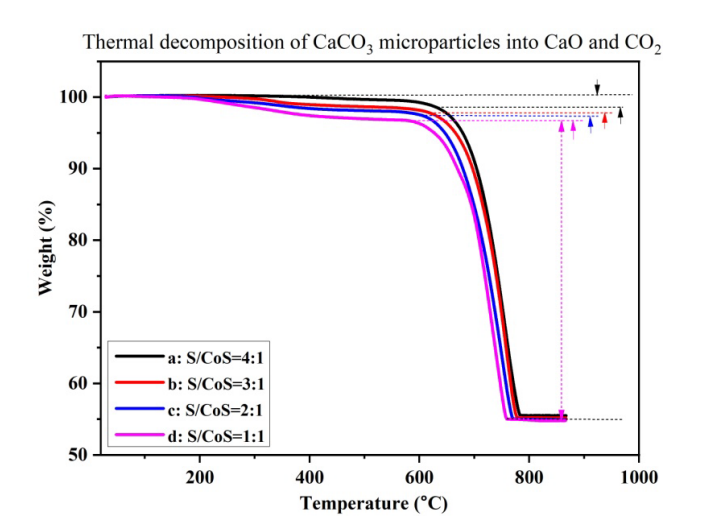


Figure 5. The TG analyses of CaCO₃ samples (a: S/CoS=4:1, b: S/CoS=3:1, c: S/CoS=2:1, d: S/CoS=1:1)

Table 1% Weight losses of CaCO₃ particles made in this study.

S/CoS	4:1	3:1	2:1	1:1
Shape	Long needle	Short needle	Elip-like	Coral-like
25°C ~ 620°C	2%	2.6%	3%	3.6%
620°C~790 °C	42.7%	42.4%	42.3%	41.8%

The weight losses varied from 41.8~42.7% when the temperature was raised thereafter from 620 °C to 790 °C. This could be attributed to the thermal decomposition of CaCO₃ into calcium oxide (CaO) and loss of CO₂, escaping from the system.

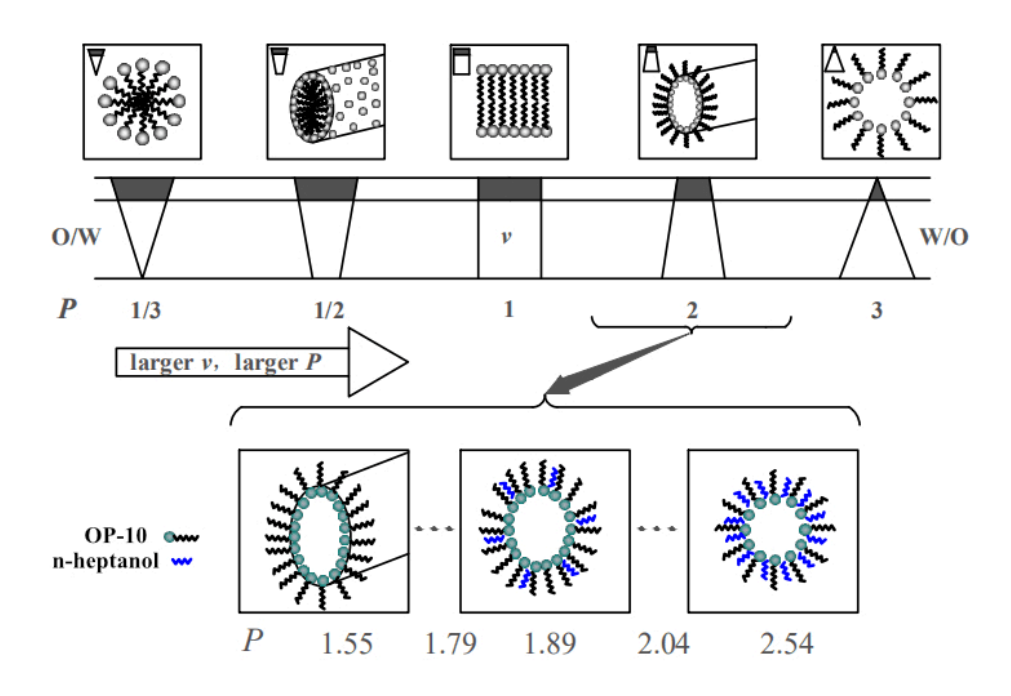
3.3. Effect of S/CoS value on the shape of reverse micelle and improved critical packing parameter theory

Experimental observations with varying S/CoS ratios suggest that the morphology of CaCO₃ microparticles is influenced by the properties of reverse micelles formed in the microemulsion. The

distribution of surfactant and cosurfactant molecules within these reverse micelles plays a significant role in determining their associative properties. This concept aligns with the theory proposed by Israelachvili *et al.*, which emphasizes the relative size of the cross-sectional areas of the hydrophilic and hydrophobic groups of surfactants in solution. Understanding this balance is crucial for comprehending how these molecular interactions impact the final morphology of the CaCO₃ microparticles. Therefore, the critical packing parameters (*P*, a parameter that predicts the surfactant's self-assembly) can be used, and it was defined as:^[46, 47]

$$P = \frac{v}{a_0 l_c} \tag{1}$$

where v is the effective volume of hydrocarbon chain, a_0 is the effective polar head group area and l_c is the fully extended length of a hydrocarbon chain. The aggregation shape of amphiphilic molecules can be speculated according to the value of P. For example, when P = 1/3, only spherical micelles exist in solution. If P = 1/2, aggregations with a rod-like shape are most likely formed. For the value P=1, there is a balance between sizes of the head group and tail, which causes the surfactant molecule forming lamellar micelle. When P=2, rod-shaped reverse micelles are formed, when P=3, spherical reverse micelles exist in solution, as shown in the upper portion of Scheme 1.



Scheme 1. Schematic diagram of the influence of n-heptanol on the *P* value of OP-10 molecule in reverse micelle.

The critical packing parameter was used to predict the properties of the surfactant. [48, 49] The nanoscale supramolecular structures composed of surfactants have been used as templates for the synthesis of inorganic materials, [50, 51] reaction field of nanoreactors, [52] modulation of wettability of biological interfaces, [53] and enhanced oil recovery from heterogeneous rocks. [54] Although the reverse micelles were also considered in the critical packing parameter theory, [46] the effect from the cosurfactant was not considered. Therefore, we here supplemented the theory by to take into account the addition of cosurfactants. Firstly, the magnitude of parameters v, l_c and a_0 can be estimated directly from quantum chemical calculations. [55, 56] Secondly, the effect of cosurfactants inserted between the surfactant in the micelles was considered. Therefore, density functional theory (DFT) calculations at the B3LYP/6-31G (d, p) level were carried out to investigate surfactant and cosurfactant molecule optimal geometric structure by Gaussian 16 software. The corresponding parameters of OP-10 are v=0.37 nm³, l_c =1.34 nm and a_0 = 0.178 nm² if no cosurfactant is present in the reverse micellular system.

When n-heptanol was introduced as a cosurfactant, the molecules are distributed in the oil-water interface layer and entered the wedge-shaped vacancy formed between OP-10, the hydroxyl group is close to the polar group of the surfactant, and its alkyl chain lies between the tail hydrocarbon chains of surfactants. These molecules assist on distribution and arrangement of surfactant molecules in the oil-water interface membrane enhance the intermolecular interaction to form stable reverse micelles, as shown in the lower part of Scheme 1. When n-heptanol molecules are inserted into the gap of OP-10 like a wedge, the consequent effect is similar as an improvement of the effective volume and cross-sectional area of the OP-10 hydrophobic tails. It also corresponded to changing the shape of surfactant from cylinder to cone, and the P value of the packing parameter will change accordingly. After the effects of cosurfactant were considered, the P values calculated are 1.79, 1.89, 2.04 and 2.54 when S/CoS = 4:1, 3:1, 2:1 and 1:1, respectively (as shown in Table 2). The results indicated that with the increase of cosurfactant, the P value increases correspondingly. This can hence be interpreted as the lower the amount of cosurfactant, the reverse micelle is close to a rod in shape, and in the presence of

more cosurfactant, the shape of the reverse micelle changes to a spherical shape.

The geometry of the reverse micelles (the shape of the micro reaction pool) will affect the final shape of the CaCO₃ particles, making their morphology similar to the shape of the micro reaction pool. Therefore, the shapes of reverse micelles change from lamellar to rod-like and then to spherical, the morphology of CaCO₃ has also undergone a transformation from lamellar, long rod, short rod, ellipsoid to spherical shape.

Table 2

The value of critical packing parameter under different S/CoS

S/CoS	1: 0	4:1	3:1	2:1	1:1
Shape	n/a	Long needle	Short needle	Elip-like	Coral-like
P	1.55	1.79	1.89	2.04	2.54

From the experimental data, when S/CoS=1:0 (without cosurfactant), microemulsion could not be formed. When S/CoS<1, stable microemulsions can not be not easily formed, this is very likely due to the overload of n-heptanol, excess alcohol molecules inserted in the surfactant molecules increase the distance and weaken the force between the surfactant molecules, hence micelles cannot be formed. Therefore, the maximum ratio of cosurfactant to surfactant should be 1:1.

According to our previous research studies [29, 57], the size of the micro reaction pool in the microemulsion $R_{\rm m}$ can be calculated according to the equation (2):

$$R_m = \frac{3(M_h V_h + M_{\text{alc}} V_{\text{alc}})}{A_S M_{\text{OP-10}}} \tag{2}$$

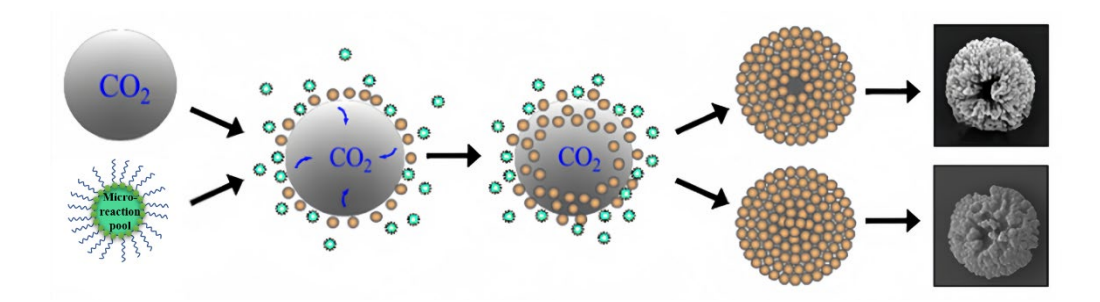
Where M_h is the molar mass of water phase, M_{alc} is the molar mass of *n*-heptanol dissolved in water, V_h is the volume of a water molecule, V_{alc} is the volume of a *n*-heptanol molecule, A_S is the cross-sectional area of surfactant OP-10, M_{OP-10} is the molar mass of OP-10.

When the volume ratio of the surfactant, cosurfactant, oil phase, and water phase is 15: 15: 50: 4, which were the conditions used for the production of coral shaped microparticles, the radius of the micro reaction pool was calculated, it is R_m =20.5 nm, therefore the diameter of the micro reaction

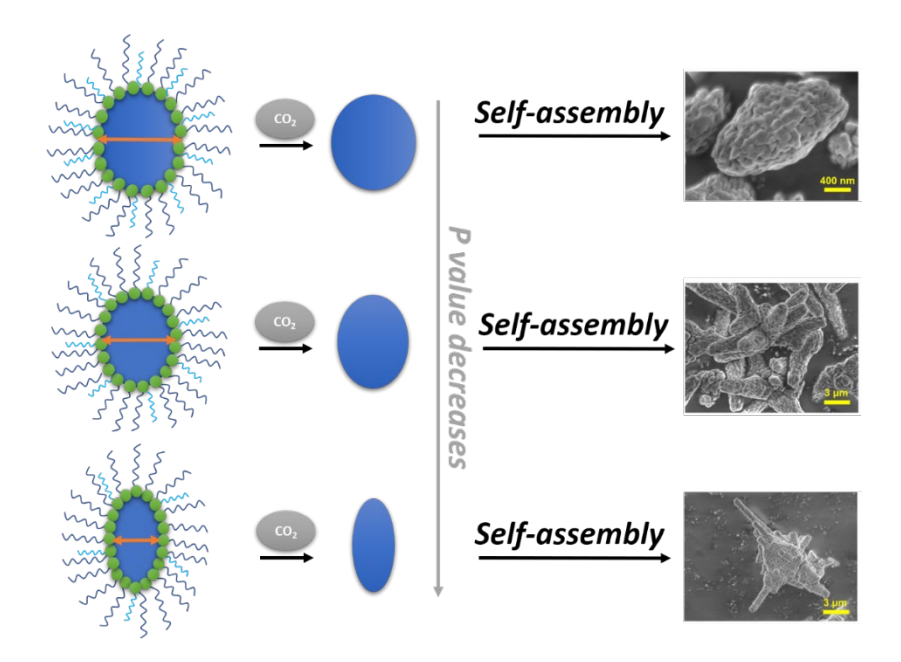
pool is D_m =41 nm. According to Figure 1, CaCO₃ particles are relatively larger micron structure, but the size of micelles calculated from the theoretical formulae should be nanometer scale. Therefore, a microstructure particle formation mechanism is proposed in the next section.

3.4. Formation mechanism of coral-like microparticles and other particular shape microparticles

In Figure 1d, the coral-like CaCO₃ microparticles appear to be composed of small CaCO₃ spherical nanoparticles. Upon measurement, the average size of these nanoparticles was found to be approximately 45 nm, closely matching the 41 nm micro reaction pool size calculated using equation (2). This observation suggests that the coral-shaped microparticles likely consist of spherical aggregations of smaller spherical nanoparticles that conform to the calculated pool volume. We propose that the formation of coral-like CaCO₃ microparticles begins with the introduction of carbon dioxide gas, leading to the formation of CaCO₃ nanoparticles due to the buildup of CO₃²⁻ ions in the pool. These CaCO₃ particles, being insoluble in water, grow in size within the pool until the surfactant can no longer stabilize them, resulting in aggregation and the formation of larger microparticles. As CO₂ continues to react with the surrounding micro reaction pools, more spherical-shaped nanoparticles are formed, which subsequently self-organize into spherical aggregates. The mechanism for this formation process is illustrated in Scheme 2. This mechanism can also explain the emergence of alternative morphologies, such as hollow raspberry-shaped and starfish-like CaCO3 particles, as depicted in Figure 2. The hollow raspberry-shaped particles may arise from an incomplete chemical reaction or possibly from the depletion of CO2 before the full development of coral-shaped microparticles. The starfish-like CaCO₃ particles appear to result from the structural collapse of some hollow coral-like CaCO₃ particles.



Scheme 2. Schematic illustration of coral-like micron calcium carbonate formation.



Scheme 3. Schematic illustration of micron calcium carbonate formation.

The formation mechanism for other shapes, such as ellipsoidal and rod-like CaCO₃ particles, closely mirrors that of coral-shaped CaCO₃ particles. However, a key difference arises with the increased ratio of surfactant to cosurfactant. This alteration causes the shape of the reverse micelles to shift from spherical to elliptical and eventually to rod-shaped, especially at progressively lower concentrations of n-heptanol. Within these evolving aqueous cavities (micelles), CO₂ reacts to form elliptical or rod-shaped nano CaCO₃ particles. Under agitated conditions, these flowing nanoscale particles then self-assemble, culminating in the formation of CaCO₃ microparticle aggregates of varying shapes, as illustrated in Scheme 3. The final shape of these aggregates is dictated by the shape of the micelles. So various experimental results were well explained by this formation mechanism.

It is important to emphasize that we have, for the first time, proposed and rationalized the formation mechanism of CaCO₃ particles in the OP-10 + n-heptanol microemulsion system. This mechanism provides a cogent explanation for the emergence of calcium carbonate particles with varied morphologies under specific conditions. Our findings offer valuable insights for the preparation of micro-nano materials within microemulsion systems. It is crucial to note that factors such as stirring rate, CO₂ bubble size, and bubble penetration rate can influence particle formation differently across various microemulsion systems. Therefore, it is possible that other systems may not yield

identical results.

3.5. The hydrophobic properties of coral-like calcium carbonate

Nowadays, many different materials were prepared to meet different needs.^[58-60] The diverse shapes of microparticles produced in this study have the potential for a wide range of applications. Notably, the coral-like CaCO₃ synthesized, as depicted in the SEM image (Figure 1d), possesses a micro-composite structure reminiscent of the surface composition of a lotus leaf. This similarity makes it a promising candidate for coating hydrophobic surfaces. Previous research indicates that the lotus leaf surface is adorned with hydrophobic nanostructures, as illustrated in Figure 6(a).^[61-63] These micro-composite structures lead to a reduced contact area and an increased contact angle between water droplets and the lotus leaf surface, endowing the leaf with remarkable superhydrophobicity and self-cleaning properties. Similarly, when micron-grade coral-like CaCO₃ particles are evenly distributed on a glass slide, they mimic the micron-sized papillae found on the lotus leaf surface. Furthermore, the nanostructures on the surface of these coral-like CaCO₃ particles closely resemble the nano-protrusions of the lotus leaf papillae. Given these structural similarities, it is intriguing to explore whether coral-like CaCO₃ might emerge as a new type of superhydrophobic material.

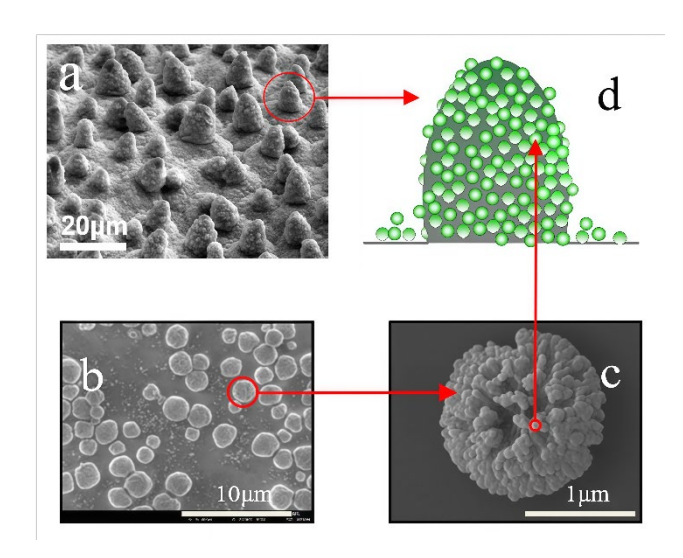


Figure 6. a) SEM image of lotus leaf surface; b) coral-like micro CaCO₃ particles image by Jeol JSM 6100 Scanning electron microscopy; c) local enlarged image of b obtained by FEI Quanta 650FEG scanning electron microscopy after ultrasonic cleaning in ethanol; d) structure sketch of lotus leaf surface.

To assess the potential of coral-like CaCO₃ microparticles for hydrophobic applications, cubic CaCO₃ microparticles were prepared based on reported procedure^[45] for a comparative contact angle analysis. The water contact angles of both cubic and coral-like CaCO₃ microparticles are presented in Figure 7. The cubic CaCO₃ microparticles, analyzed via XRD, were found to consist of a mixture of calcite and vaterite. In comparison, the contact angle for the cubic CaCO3 particles was measured at 51.6°, whereas the coral-like CaCO₃ sample exhibited a higher angle of 76.3°, consistent with our previous measurements. This indicates that, although the large surface area of the microparticles was coated with surfactants, the hydrophobic effect exhibited was limited. Therefore, to enhance their hydrophobic properties, both coral-like and cubic CaCO₃ particles were further modified with stearic acid. This modification aimed to optimize their hydrophobicity and improve their suitability for waterrepellent applications. After surface modification, both coral-like and cubic CaCO₃ particles were coated onto glass slides. The contact angle measurements revealed that the modified cubic CaCO₃ particles exhibited a contact angle of 127.1°, as shown in Figure 7c. In contrast, the coral-like CaCO₃ microparticles displayed a higher contact angle of 137.3°, as depicted in Figure 7d. The contact angles of CaCO₃ coating before and after stearic acid modification were listed in Table 3. This finding indicates that the coral-like CaCO₃ microparticles possess superior hydrophobic properties compared to their cubic counterparts, both before and after surface modification with steric acid. The enhanced hydrophobicity of the coral-like particles can be attributed to their larger surface area, which allows for greater accommodation of stearic acid. These results are in line with our theoretical model and corroborate observations from previous research.

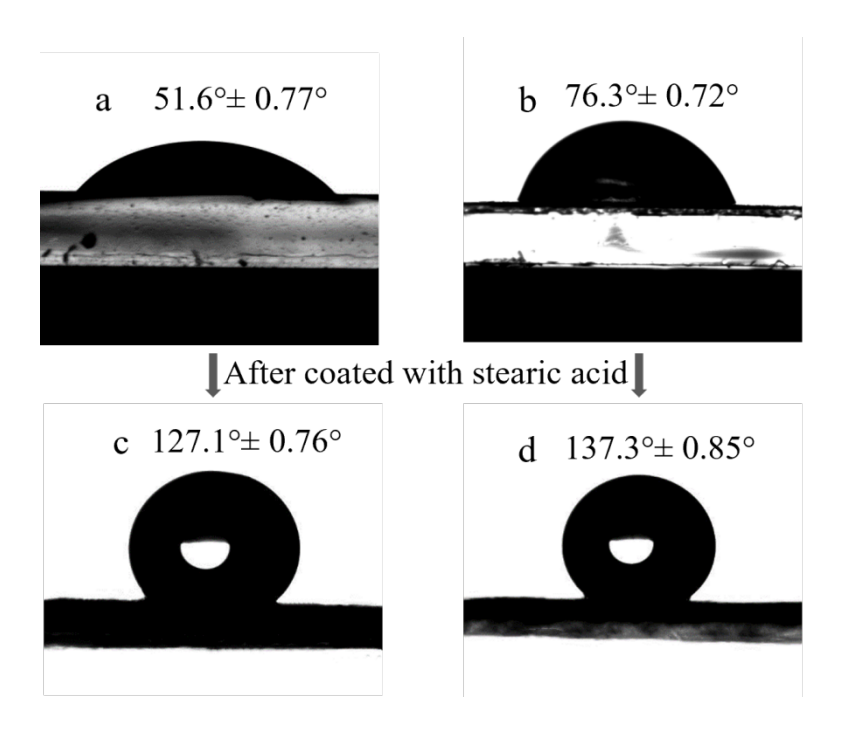


Figure 7. Contact angle images of water droplets on different morphology CaCO₃ particles coatings. a) cubic CaCO₃ microparticles; b) coral-like CaCO₃ microparticles; c) cubic CaCO₃ microparticles modified by stearic acid; d) coral-like CaCO₃ microparticles modified by stearic acid.

Table 3Contact angles of CaCO₃ coating before and after stearic acid modification.

	Before	Modifier	After
coral-like calcium carbonate	76.3°±0.72°	stearic acid	137.3°± 0.9°
cubic calcium carbonate	51.6°±0.77°	stearic acid	127.1°± 0.8°

4. Conclusion

In this research, diverse morphologies of CaCO₃ microparticles were prepared by adjusting the volumetric ratio between surfactant and cosurfactant (S/CoS) in an inverse microemulsion. It was observed that this ratio significantly influences the final morphology and size of the CaCO₃ microparticles. To decipher the formation process, the critical packing parameters theory was employed and further developed for this microemulsion system. Our proposed mechanism suggests

that reverse micelles, varying in S/CoS ratios, initially react with CO2 bubbles to form CaCO3

nanoparticles of different shapes, which subsequently self-assemble into microparticles with varied

morphologies. Future studies aim to utilize cryoelectron microscopy to confirm this nano-to-

microparticle growth process. In a practical demonstration, coral-like CaCO₃ microparticles were

modified with stearic acid and then deposited onto a glass slide. This modification markedly improved

the contact angle, endowing the surface with properties similar to the microdomains of a lotus leaf and

exhibiting exceptional hydrophobic characteristics. These findings open avenues for a variety of

surface coating applications. For example, modified microparticles can be used for surface protection,

emulating the water-repellent qualities of a lotus leaf. Covering a surface with these microparticles

could create a pattern of water-repelling features, akin to the lotus leaf's microstructure. Another

promising application is the deposition of these microparticles onto metal surfaces, followed by a

stearic acid wash. This technique could form a protective hydrophobic layer, effectively guarding the

metal against corrosion. Such strategies not only promise to enhance the durability of metal surfaces

but also capitalize on the unique characteristics of these microparticles for innovative material

coatings.

Acknowledgements

This work was supported by the Key Technology and Industrial Application Demonstration Project

of High Quality and High Purity Nano Calcium Carbonate of Guangxi Province (Grant No.

17202030-2) and the Gansu Province Key Research and Development Program (Grant No.

23YFGA0044).

Conflict of interest

The authors declare that they have no conflict of interest.

Author contributions

Conceptualization: Nong Wang, Zhihang Wang, Martyn Jevric

Formal analysis: Meikun Hu, Ke Wang

Investigation: Meikun Hu, Ke Wang, Jiajun Zuo, Jiaming Feng

20

Methodology: Nong Wang, Jiaming Feng

Resources: Nong Wang

Supervision: Nong Wang

Project administration: Nong Wang

Writing - original draft: Meikun Hu, Zhihang Wang, Martyn Jevric

Writing - review & editing: Nong Wang, Zhihang Wang, Martyn Jevric

All authors have read and approved the final version to be published.

References

- [1] M. Chaussemier, E. Pourmohtasham, D. Gelus, N. Pécoul, H. Perrot, J. Lédion, H. Cheap-Charpentier, O. Horner, "State of art of natural inhibitors of calcium carbonate scaling. A review article" *Desalination* **2015**, *356*, 47-55.
- [2] C. A. Schmidt, E. Tambutte, A. A. Venn, Z. Zou, C. Castillo Alvarez, L. S. Devriendt, H. A. Bechtel, C. A. Stifler, S. Anglemyer, C. P. Breit, C. L. Foust, A. Hopanchuk, C. N. Klaus, I. J. Kohler, I. M. LeCloux, J. Mezera, M. R. Patton, A. Purisch, V. Quach, J. S. Sengkhammee, T. Sristy, S. Vattem, E. J. Walch, M. Alberic, Y. Politi, P. Fratzl, S. Tambutte, P. Gilbert, "Myriad Mapping of nanoscale minerals reveals calcium carbonate hemihydrate in forming nacre and coral biominerals" *Nat. Commun.* **2024**, *15*, 1812.
- [3] N. K. Dhami, M. E. C. Quirin, A. Mukherjee, "Carbonate biomineralization and heavy metal remediation by calcifying fungi isolated from karstic caves" *Ecol. Eng.* **2017**, *103*, 106-117.
- [4] H. Lu, H. Lutz, S. J. Roeters, M. A. Hood, A. Schäfer, R. Muñoz-Espí, R. Berger, M. Bonn, T. Weidner, "Calcium-Induced Molecular Rearrangement of Peptide Folds Enables Biomineralization of Vaterite Calcium Carbonate" *J. Am. Chem. Soc.* **2018**, *140*, 2793-2796.
- [5] F. C. Meldrum, "Calcium carbonate in biomineralisation and biomimetic chemistry" *Int. Mater. Rev.* **2013**, *48*, 187-224.
- [6] D. Yang, Y. Yan, X. Yang, J. Liu, G. Zheng, L. Xie, R. Zhang, "A basic protein, N25, from a mollusk modifies calcium carbonate morphology and shell biomineralization" *J. Biol. Chem.* **2019**, *294*, 8371-8383.
- [7] S. Sovova, A. Abalymov, M. Pekar, A. G. Skirtach, B. Parakhonskiy, "Calcium carbonate particles: synthesis, temperature and time influence on the size, shape, phase, and their impact on cell hydroxyapatite formation" *J. Mater. Chem. B* **2021**, *9*, 8308-8320.
- [8] B. Jin, S. Wang, Y. Lei, H. Jia, Q. Niu, M. F. Dapaah, Y. Gao, L. Cheng, "Green and effective remediation of heavy metals contaminated water using CaCO₃ vaterite synthesized through biomineralization" *J. Environ. Manage.* **2024**, *353*, 120136.
- [9] P. J. M. Smeets, K. R. Cho, R. G. E. Kempen, N. A. J. M. Sommerdijk, J. J. De Yoreo, "Calcium carbonate nucleation driven by ion binding in a biomimetic matrix revealed by in situ electron microscopy" *Nat. Mater.* **2015**, *14*, 394-399.
- [10] C. R. M. e. Portugal, C. Fonyo, C. C. Machado, R. Meganck, T. Jarvis, "Microbiologically Induced Calcite Precipitation biocementation, green alternative for roads is this the breakthrough? A critical review" *J. Clean. Prod.* **2020**, *262*, 121372.
- [11] B. M. M. Soledad Fernández, Liliana Ortiz, Andrónico Neira-Carrillo, José Luis Arias, "Effect of Carbonic Anhydrase Immobilized on Eggshell Membranes on Calcium Carbonate Crystallization In Vitro", *Singapore* **2018**. [12] N. Phuhiangpa, S. Phongphanphanee, W. Smitthipong, "Study of rubber/calcium carbonate composites" *IOP Conf. Ser.: Mater. Sci. Eng.* **2020**, *773*, 012013.
- [13] H. Sadeghi Ghari, A. Jalali-Arani, "Nanocomposites based on natural rubber, organoclay and nano-calcium carbonate: Study on the structure, cure behavior, static and dynamic-mechanical properties" *Appl. Clay Sci.* **2016**, *119*, 348-357.

- [14] T. Thenepalli, A. Y. Jun, C. Han, C. Ramakrishna, J. W. Ahn, "A strategy of precipitated calcium carbonate (CaCO₃) fillers for enhancing the mechanical properties of polypropylene polymers" *Korean J. Chem. Eng.* **2015**, 32, 1009-1022.
- [15] Y. Mori, A. Isogai, T. Enomae, "Application of Vaterite-Type Calcium Carbonate Prepared by Ultrasound for Ink Jet Paper" *J. Imaging Sci. Technol.* **2010**, *54*, 20504-20506.
- [16] A. M. Atta, H. A. Al-Lohedan, A. O. Ezzat, S. A. Al-Hussain, "Characterization of superhydrophobic epoxy coatings embedded by modified calcium carbonate nanoparticles" *Prog. Org. Coat.* **2016**, *101*, 577-586.
- [17] C. Muderrisoglu, M. Saveleva, A. Abalymov, L. Van der Meeren, A. Ivanova, V. Atkin, B. Parakhonskiy, A. G. Skirtach, "Nanostructured Biointerfaces Based on Bioceramic Calcium Carbonate/Hydrogel Coatings on Titanium with an Active Enzyme for Stimulating Osteoblasts Growth" *Adv. Mater. Interfaces* **2018**, *5*, 1800452.
- [18] R. Gaudreault, N. Di Cesare, T. G. M. van de Ve, D. A. Weitz, "Structure and Strength of Flocs of Precipitated Calcium Carbonate Induced by Various Polymers Used in Papermaking" *Ind. Eng. Chem. Res.* **2015**, *54*, 6234-6246.
- [19] B. Cheng, M. Lei, J. Yu, X. Zhao, "Preparation of monodispersed cubic calcium carbonate particles via precipitation reaction" *Mater. Lett.* **2004**, *58*, 1565-1570.
- [20] H. Saulat, M. Cao, M. M. Khan, M. Khan, M. Khan, A. Rehman, "Preparation and applications of calcium carbonate whisker with a special focus on construction materials" *Constr. Build. Mater.* **2020**, *236*, 117613.
- [21] Y. Mori, T. Enomae, A. Isogai, "A Preparation of Spherical Calcium Carbonate and Application to Paper" *Proc. of IS&T's NIP.* **2005**, *21*, 457-460.
- [22] S. Palsule, Polymers and polymeric composites: a reference series(Eds.), Springer. 2016.
- [23] D. B. Trushina, S. N. Sulyanov, T. V. Bukreeva, M. V. Kovalchuk, "Size control and structure features of spherical calcium carbonate particles" *Crystallogr. Rep.* **2015**, *60*, 570-577.
- [24] J. S. Cho, Y. N. Ko, H. Y. Koo, Y. C. Kang, "Synthesis of nano-sized biphasic calcium phosphate ceramics with spherical shape by flame spray pyrolysis" *J. Mater. Sci.: Mater. Med.* **2010**, *21*, 1143-1149.
- [25] Ç. M. Oral, A. Çalışkan, Y. Göçtü, D. Kapusuz, B. Ercan, "Synthesis of calcium carbonate microspheres via inert gas bubbling for orthopedic applications" *Ceram. Int.* **2020**, *46*, 3513-3522.
- [26] D. B. Trushina, T. N. Borodina, S. Belyakov, M. N. Antipina, "Calcium carbonate vaterite particles for drug delivery: Advances and challenges" *Mater. Today. Adv.* **2022**, *14*, 100214.
- [27] L. Minkowicz, A. Dagan, V. Uvarov, O. Benny, "Controlling Calcium Carbonate Particle Morphology, Size, and Molecular Order Using Silicate" *Materials* **2021**, *14*, 3525.
- [28] N. Wang, Q. L. Meng, "Study of the Influence between Barium Ions and Calcium Ions on Morphology and Size of Coprecipitation in Microemulsion" *Surf. Rev. Lett.* **2015**, *22*, 1550036.
- [29] N. Wang, X. Wang, L. Yang, H. Chen, "Morphology and size control of nanocalcium carbonate crystallised in reverse micelle system with cationic surfactant cetyltrimethylammonium bromide" *Micro Nano Lett.* **2013**, *8*, 94-98.
- [30] N. Wang, L. Yang, L. Che, R. Xiao, "Study of the influence between magnesium ions and calcium ions on the morphology and size of coprecipitation in microemulsion" *Micro Nano Lett.* **2014**, *9*, 302-307.
- [31] D. J. McClements, Food emulsions: principles, practices, and techniques, Third Edition (3rd ed.), CRC Press. 2015.
- [32] D. Arab, A. Kantzas, S. L. Bryant, "Nanoparticle stabilized oil in water emulsions: A critical review" *J.Pet. Eng.* **2018**, *163*, 217-242.
- [33] M. Fingas, "Water-in-oil emulsion formation: A review of physics and mathematical modelling" *Spill Sci. Technol Bull.* **1995**, *2*, 55-59.
- [34] A. Benichou, A. Aseri, N. Garti, "Double emulsions stabilized with hybrids of natural polymers for entrapment and slow release of active matters" *Adv. Colloid Interface Sci.* **2004**, *108-109*, 29-41.
- [35] S. Vandergraaf, C. Schroen, R. Boom, "Preparation of double emulsions by membrane emulsification-a review" *J. Membr. Sci.* **2005**, *251*, 7-15.
- [36] Z. Fan, B. Bhandari, "Encapsulation of polyphenols a review" Trends Food Sci. Technol. 2010, 21, 510-523.
- [37] T. Tadros, P. Izquierdo, J. Esquena, C. Solans, "Formation and stability of nano-emulsions" *Adv. Colloid Interface Sci.* **2004**, *108-109*, 303-318.
- [38] T. G. Mason, "Emulsiogenesis and the Emergence of Nanoemulsions" Matter 2019, 1, 542-546.
- [39] H. Xue, Y. Han, G. Liu, W. Chen, Z. Wang, N. Wang, "Photoresponsive surfactants for controllable and reversible emulsion systems" *Colloid Surface. A* **2025**, *705*, 135669.
- [40] S. T. Preksha Fadia, Stuti Bhagat, Abhishek Nair, Pooja Panchal, Harsh Dave, Sadev Dang, Sanjay Singh, "Calcium carbonate nano- and microparticles: synthesis methods and biological applications" *3 Biotech* **2021**, 457.

- [41] Y. Wang, L. Jiang, B. Li, Y. Ma, Y. Zeng, D. Yu, N. Wang, "Superhydrophobic fluorescent micro-/nano-composites from carbon dots encapsulated in CaCO₃-SiO₂" *Compos. Interfaces* **2023**, *31*, 401-415.
- [42] R. P. Bagwe, C. Yang, L. R. Hilliard, W. Tan, "Optimization of Dye-Doped Silica Nanoparticles Prepared Using a Reverse Microemulsion Method" *Langmuir* **2004**, *20*, 8336-8342.
- [43] Y. Ding, Y. Liu, Y. Ren, H. Yan, M. Wang, D. Wang, X.-Y. Lu, B. Wang, T. Fan, H. Guo, "Controllable synthesis of all the anhydrous CaCO₃ polymorphs with various morphologies in CaCl₂-NH₃-CO₂ aqueous system" *Powder Technol.* **2018**, *333*, 410-420.
- [44] Y. Boyjoo, V. K. Pareek, J. Liu, "Synthesis of micro and nano-sized calcium carbonate particles and their applications" *J. Mater. Chem. A* **2014**, *2*, 14270-14288.
- [45] Y. Ma, P. Tian, M. Bounmyxay, Y. Zen, N. Wang, "Calcium Carbonate@silica Composite with Superhydrophobic Properties" *Molecules* **2021**, *26*, 7180.
- [46] J. Israelachvili, "The science and applications of emulsions—an overview" Colloid Surface. A 1994, 91, 1-8.
- [47] J. Israelachvili, "Self-Assembly in Two Dimensions: Surface Micelles and Domain Formation in Monolayers" *Langmuir* **2002**, *10*, 3774-3781.
- [48] R. Nagarajan, "Molecular Packing Parameter and Surfactant Self-Assembly: The Neglected Role of the Surfactant Tail" *Langmuir* **2002**, *18*, 31-38.
- [49] A. V. Singh, Z. Hosseinidoust, B. W. Park, O. Yasa, M. Sitti, "Microemulsion-Based Soft Bacteria-Driven Microswimmers for Active Cargo Delivery" *ACS Nano* **2017**, *11*, 9759-9769.
- [50] T. Miyazawa, K. Matsuda, A. Fujimori, Y. Nonomura, "One-pot Synthesis of Manganese Oxide Nanoparticles from Microemulsion Systems" *Chem. Lett.* **2011**, *40*, 1262-1263.
- [51] Z.-R. Tian, W. Tong, J.-Y. Wang, N.-G. Duan, V. V. Krishnan, S. L. Suib, "Manganese Oxide Mesoporous Structures: Mixed-Valent Semiconducting Catalysts" *Science* **1997**, *276*, 926-930.
- [52] M. J. Thiele, M. D. Davari, I. Hofmann, M. Konig, C. G. Lopez, L. Vojcic, W. Richtering, U. Schwaneberg, L. A. Tsarkova, "Enzyme-Compatible Dynamic Nanoreactors from Electrostatically Bridged Like-Charged Surfactants and Polyelectrolytes" *Angew. Chem. Int. Ed. Engl.* **2018**, *57*, 9402-9407.
- [53] P. Boonme, "Applications of microemulsions in cosmetics." J. Cosmet. Dermatol. 2017, 6, 223–228.
- [54] T. Qin, L. Goual, M. Piri, Z. Hu, D. Wen, "Nanoparticle-stabilized microemulsions for enhanced oil recovery from heterogeneous rocks" *Fuel* **2020**, *274*, 117830.
- [55] S. Du, N. Yao, S. Liu, Y. Xu, J. Cao, W. Zhuang, J. Yu, N. Wang, D. Yu, F. Zhan, E. Wang, "Nonfullerene acceptors from thieno[3,2-b]thiophene-fused naphthalene donor core with six-member-ring connection for efficient organic solar cells" *Dyes Pigm.* **2021**, *185*, 108892.
- [56] R. A. Khalil, A.-h. A. Zarari, "Theoretical estimation of the critical packing parameter of amphiphilic self-assembled aggregates" *Appl. Surf. Sci.* **2014**, *318*, 85-89.
- [57] T. Zhao, C. Xu, Y. Ma, Y. Zen, N. Wang, "Study on preparation and structure of chrysanthemum-shaped micron calcium carbonate based on inverse microemulsion" *Micro Nano Lett.* **2020**, *15*, 1151-1155.
- [58] Q. Zhang, H. Wang, L. Qiu, X. Han, Z. Wang, N. Wang, "Synthesis and Characteristics of Smart Coating Materials for Reversible Double Stimulus-Responsive Oil–Water Separation" *ACS Appl. Polym. Mater* **2024**, *6*, 6482-6494.
- [59] X. Yu, H. Li, X. Gao, M. Chhattal, Q. Zheng, W. Wu, Z. Gong, N. Wang, J. Liu, "Effect of Heavy Ion Irradiation on Friction of GNSs: Implications for Aerospace Lubrication" *ACS Appl. Polym. Mater.* **2024**, *7*, 12035-12042.
- [60] Q. Zhang, W. Chen, J. Zuo, G. Liu, X. Han, N. Wang, "Fish Scale-Inspired beta-Cyclodextrin Cross-Linked Polyacrylamide Hydrogels for Oil-Water Separation" *ACS Appl. Mater. Interfaces* **2025**, *17*, 17389-17397.
- [61] H. J. Ensikat, P. Ditsche-Kuru, C. Neinhuis, W. Barthlott, "Superhydrophobicity in perfection: the outstanding properties of the lotus leaf" *Beilstein J. Nanotechnol.* **2011**, *2*, 152-161.
- [62] K. Koch, A. Dommisse, W. Barthlott, "Chemistry and Crystal Growth of Plant Wax Tubules of Lotus (Nelumbo nucifera) and Nasturtium (Tropaeolum majus) Leaves on Technical Substrates" *Cryst. Growth Des.* **2006**, *6*, 2571-2578.
- [63] J. Wang, H. Chen, T. Sui, A. Li, D. Chen, "Investigation on hydrophobicity of lotus leaf: Experiment and theory" *Plant Sci. (Amsterdam, Neth.)* **2009**, *176*, 687-695.